Discrete-dipole approximation for periodic targets: theory and tests

Bruce T. Draine[1,*] and Piotr J. Flatau[2]

[1]*Princeton University Observatory, Princeton, New Jersey 08544-1001, USA*
[2]*Scripps Institution of Oceanography, University of California San Diego, La Jolla, California 92093, USA*
[*]*Corresponding author: draine@astro.princeton.edu*

Received June 24, 2008; accepted August 19, 2008;
posted September 3, 2008 (Doc. ID 97834); published October 14, 2008

The discrete-dipole approximation (DDA) is a powerful method for calculating absorption and scattering by targets that have sizes smaller than or comparable to the wavelength of the incident radiation. The DDA can be extended to targets that are singly or doubly periodic. We generalize the scattering amplitude matrix and the 4×4 Mueller matrix to describe scattering by singly and doubly periodic targets and show how these matrices can be calculated using the DDA. The accuracy of DDA calculations using the open-source code DDSCAT is demonstrated by comparison with exact results for infinite cylinders and infinite slabs. A method for using the DDA solution to obtain fields within and near the target is presented, with results shown for infinite slabs.

OCIS codes: 050.1755, 050.5298, 260.0260, 290.5825.

1. INTRODUCTION

Electromagnetic scattering is used to study isolated particles, but increasingly to characterize extended targets ranging from nanostructure arrays in laboratories to planetary and asteroidal regoliths. To model the absorption and scattering, Maxwell's equations must be solved for the target geometry.

For scattering by isolated particles with complex geometry, a number of different theoretical approaches have been used, including the discrete-dipole approximation (DDA) [1–4], also known as the coupled-dipole approximation or coupled-dipole method. The DDA can treat inhomogeneous targets and anisotropic materials, and has been extended to treat targets near substrates [5,6]. Other techniques have also been employed, including the finite-difference time-domain (FDTD) method [7,8].

For illumination by monochromatic plane waves, the DDA can be extended to targets that are spatially periodic and (formally) infinite in extent. This could apply, for example, to a periodic array of nanostructures in a laboratory setting, or it might be used to approximate a regolith by a periodic array of "target unit cells" with complex structure within each unit cell.

Generalization of the DDA (or coupled-dipole method) to periodic structures was first presented by Markel [9] for a 1-dimensional chain of dipoles, and more generally by Chaumet *et al.* [10], who calculated the electric field near a 2-dimensional array of parallelepipeds illuminated by a plane wave. Chaumet and Sentenac [11] further extended the DDA to treat periodic structures with a finite number of defects.

From a computational standpoint, solving Maxwell's equations for periodic structures is only slightly more difficult than calculating the scattering properties of a single "unit cell" from the structure. Since it is now feasible to treat targets with $N\gtrsim10^6$ dipoles (target volume $\gtrsim200\lambda^3$, where λ is the wavelength), it becomes possible to treat extended objects with complex substructure.

The objective of the present paper is to present the theory of the DDA applied to scattering and absorption by structures that are periodic in one or two spatial dimensions. We also generalize the standard formalism for describing the far-field scattering properties of finite targets (the 2×2 scattering amplitude matrix and 4×4 Mueller matrix) to describe scattering by periodic targets. We show how to calculate the Mueller matrix to describe scattering of arbitrarily polarized radiation. The theoretical treatment developed here has been implemented in the open-source code DDSCAT 7 (see Appendix A).

The theory of the DDA for periodic targets is reviewed in Section 2, and the formalism for describing the far-field scattering properties of periodic targets is presented in Sections 3–5. Transmission and reflection coefficients for targets that are periodic in two dimensions are obtained in Section 6.

The applicability and accuracy of the DDA method are discussed in Sections 7 and 8, where we show scattering properties calculated using DDSCAT 7 for two geometries for which exact solutions are available for comparison: (1) an infinite cylinder and (2) an infinite slab of finite thickness. The numerical comparisons demonstrate that, for given λ, the DDA converges to the exact solution as the interdipole spacing $d\rightarrow0$.

2. DDA FOR PERIODIC TARGETS

The DDA is a general technique for calculating scattering and absorption of electromagnetic radiation by targets with arbitrary geometry. The basic theory of the DDA has been presented elsewhere [3]. Conceptually, the DDA consists of approximating the target of interest by an array of polarizable points with specified polarizabilities. Once the

polarizabilities are specified, Maxwell's equations can be solved accurately for the dipole array. When applied to finite targets, the DDA is limited by the number of dipoles N for which computations are feasible—the limitations may arise from large memory requirements or the large amount of computing that may be required to find a solution when N is large. In practice, modern desktop computers are capable of solving the DDA equations, as implemented in DDSCAT [3,12], for N as large as $\sim 10^6$.

Developed originally to study scattering from isolated, finite structures such as dust grains [1], the DDA can be extended to treat singly or doubly periodic structures. Consider a collection of N polarizable points defining a target unit cell (TUC). Now consider a target consisting of a 1-dimensional or 2-dimensional periodic array of identical TUCs, as illustrated in Figs. 1 and 2; we will refer to these as 1-D or 2-D targets, although the constituent TUC may have an arbitrary 3-dimensional shape. For a monochromatic incident plane wave

$$\mathbf{E}_{\rm inc}(\mathbf{r},t) = \mathbf{E}_0 \exp(i\mathbf{k}_0 \cdot \mathbf{r} - i\omega t), \quad (1)$$

the polarizations of the dipoles in the target will oscillate coherently. Each dipole will be affected by the incident wave plus the electric field generated by *all* of the other point dipoles.

Let index $j=1,\ldots,N$ run over the dipoles in a single TUC, and let indices m, n run over replicas of the TUC. The (m,n) replica of dipole j is located at

$$\mathbf{r}_{jmn} = \mathbf{r}_{j00} + m\mathbf{L}_u + n\mathbf{L}_v, \quad (2)$$

where $\mathbf{L}_u$ and $\mathbf{L}_v$ are the lattice vectors for the array. For 1-D targets we let m vary, but set $n=0$. For 2-D targets, the area per TUC is

$$A_{\rm TUC} \equiv |\mathbf{L}_u \times \mathbf{L}_v| = L_u L_v \sin\theta_{uv}, \quad (3)$$

where θ_{uv} is the angle between $\mathbf{L}_u$ and $\mathbf{L}_v$.

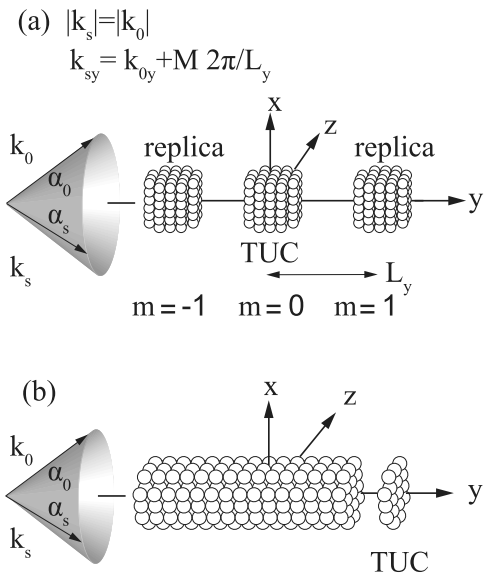

Fig. 1. (a) Target consisting of a 1-D array of TUCs and (b) showing how an infinite cylinder can be constructed from disk-like TUCs (lower). The $M=0$ scattering cone with $\alpha_s=\alpha_0$ is illustrated.

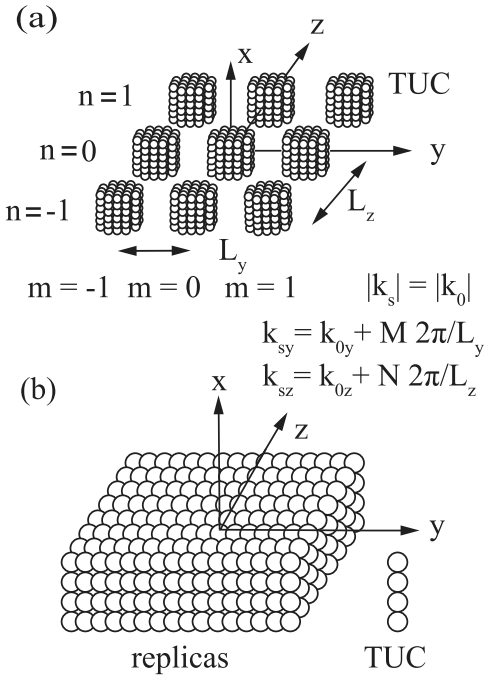

Fig. 2. (a) Target consisting of a 2-D array of TUCs and (b) showing how an infinite slab is created from TUCs consisting of a single "line" of dipoles.

The replica dipole polarization $\mathbf{P}_{jmn}(t)$ is phase-shifted relative to $\mathbf{P}_{j00}(t)$:

$$\mathbf{P}_{jmn}(t) = \mathbf{P}_{j00}(t)\exp[i(m\mathbf{k}_0 \cdot \mathbf{L}_u + n\mathbf{k}_0 \cdot \mathbf{L}_v)]. \quad (4)$$

Define a matrix $\mathbf{A}$ such that $-\mathbf{A}_{j,kmn}\mathbf{P}_{kmn}$ gives the electric field $\mathbf{E}$ at $\mathbf{r}_{j00}$ produced by an oscillating dipole $\mathbf{P}_{kmn}$ located at $\mathbf{r}_{kmn}$. Expressions for the 3×3 tensor elements of $\mathbf{A}$ have been presented elsewhere (e.g., [3]); $\mathbf{A}$ depends on the target geometry and wavelength of the incident radiation, but not on the target composition nor on the direction or polarization state of the incident wave.

Using Eq. (2) we may construct a matrix $\tilde{\mathbf{A}}$ such that, for $j \neq k$, $-\tilde{\mathbf{A}}_{j,k}\mathbf{P}_{k00}$ gives the electric field at $\mathbf{r}_{j00}$ produced by a dipole $\mathbf{P}_{k00}$ and all of its replica dipoles $\mathbf{P}_{kmn}$, and for $j=k$ it gives the electric field at $\mathbf{r}_{j00}$ produced only by the replica dipoles:

$$\tilde{\mathbf{A}}_{j,k} = \sum_{m=-\infty}^{\infty} \sum_{n=-n_{\rm max}}^{n_{\rm max}} (1-\delta_{jk}\delta_{m0}\delta_{n0})\mathbf{A}_{j,kmn} \exp[i(m\mathbf{k}_0 \cdot \mathbf{L}_u + n\mathbf{k}_0 \cdot \mathbf{L}_v)], \quad (5)$$

where $n_{\rm max}=0$ for 1-D targets and $n_{\rm max}=\infty$ for 2-D targets, and δ_{ij} is the Kronecker delta. For $|m|,|n| \to \infty$, location $j00$ is in the radiation zone of dipole kmn, and the electric field falls off in magnitude only as $1/r$. The sums in Eq. (5) would be divergent were it not for the oscillating phases of the terms, which ensure convergence. Evaluation of these sums can be computationally demanding when $k_0 L_y$ or $k_0 L_z$ are small. Chaumet *et al.* [10] have discussed methods for efficient evaluation of these sums.

We evaluate Eq. (5) numerically by introducing a factor $\exp[-(\gamma k_0 r)^4]$ to smoothly suppress the contributions from large r, and truncating the sums:

$$\tilde{\mathbf{A}}_{j,k} \approx \sum_{m,n}{}' \mathbf{A}_{j,kmn} \exp[i(m\mathbf{k}_0\cdot\mathbf{L}_u + n\mathbf{k}_0\cdot\mathbf{L}_v) - (\gamma k_0 r_{j,kmn})^4], \tag{6}$$

where $r_{j,kmn}\equiv|\mathbf{r}_{kmn}-\mathbf{r}_{j00}|$ and the summation is over (m,n) with $r_{j,kmn}\leq 2/\gamma k_0$, i.e., out to distances where the suppression factor $\exp[-(\gamma k_0 r)^4]\approx e^{-16}$. For given $\mathbf{k}_0$, $\mathbf{L}_u$, $\mathbf{L}_v$, the $\tilde{\mathbf{A}}_{j,k}$ depend only on $\mathbf{r}_{j00}-\mathbf{r}_{k00}$, and therefore only $O(8N)$ distinct $\tilde{\mathbf{A}}_{j,k}$ require evaluation.

Ideally, one would use a very small value for the interaction cutoff parameter γ, but the number of terms [$\propto\gamma^{-1}$ for 1-D or $\propto\gamma^{-2}$ for 2-D] in Eq. (6) diverges as $\gamma\to 0$. We show that setting $\gamma\approx 0.001$ ensures accurate results for the cases studied here.

The polarizations $\mathbf{P}_{j00}$ of the dipoles in the TUC must satisfy the system of equations

$$\mathbf{P}_{j00} = \boldsymbol{\alpha}_j\left[\mathbf{E}_{\rm inc}(\mathbf{r}_j) - \sum_{k\neq j}\tilde{\mathbf{A}}_{j,k}\mathbf{P}_{k00}\right]. \tag{7}$$

If there are N dipoles in one TUC, then Eq. (7) is a system of $3N$ linear equations where the polarizability tensors α_j are obtained from lattice-dispersion-relation theory [13,14]. After $\tilde{\mathbf{A}}$ has been calculated, Eq. (7) can be solved for $\mathbf{P}_{j00}$ using iterative techniques when $N\gg 1$.

3. IN THE RADIATION ZONE

In the radiation zone $kr\gg 1$, the electric field due to dipole jmn is

$$\mathbf{E}_{jmn} = \frac{k_0^2\exp(ik_0|\mathbf{r}-\mathbf{r}_{jmn}|)}{|\mathbf{r}-\mathbf{r}_{jmn}|}\left[1-\frac{(\mathbf{r}-\mathbf{r}_{jmn})(\mathbf{r}-\mathbf{r}_{jmn})}{|\mathbf{r}-\mathbf{r}_{jmn}|^2}\right]\mathbf{P}_{jmn}, \tag{8}$$

$$|\mathbf{r}-\mathbf{r}_{jmn}| = [r^2 - 2\mathbf{r}\cdot\mathbf{r}_{jmn} + r_{jmn}^2]^{1/2} \approx r\left\{1-\frac{\mathbf{r}\cdot\mathbf{r}_{jmn}}{r^2} + \frac{1}{2r^2}\left[r_{jmn}^2 - \left(\frac{\mathbf{r}\cdot\mathbf{r}_{jmn}}{r}\right)^2\right] + \cdots\right\}. \tag{9}$$

Define the unit vector $\hat{\mathbf{k}}_s\equiv\mathbf{k}_s/k_0$. We seek to sum the contribution of all the dipoles to the electric field propagating in direction $\hat{\mathbf{k}}_s$. At location $\mathbf{r}=r\hat{\mathbf{k}}_s$, the dominant contribution will be from dipoles located within the Fresnel zone (see, e.g., [15]), which will have a transverse radius $R_F\approx(r/k_0)^{1/2}$. For dipoles within the Fresnel zone,

$$\frac{1}{|\mathbf{r}-\mathbf{r}_{jmn}|}\left[1-\frac{(\mathbf{r}-\mathbf{r}_{jmn})(\mathbf{r}-\mathbf{r}_{jmn})}{|\mathbf{r}-\mathbf{r}_{jmn}|^2}\right]\mathbf{P}_{jmn} \approx \frac{1}{r}[1-\hat{\mathbf{k}}_s\hat{\mathbf{k}}_s]\mathbf{P}_{jmn}. \tag{10}$$

Thus, in the radiation zone,

$$\mathbf{E}(\mathbf{r}) = \frac{k_0^3}{k_0 r}\exp(ik_0 r)[1-\hat{\mathbf{k}}_s\hat{\mathbf{k}}_s]\sum_j\mathbf{P}_{j00}\sum_{m,n}\exp(i\psi_{jmn}), \tag{11}$$

with

$$\psi_{jmn} \equiv m\mathbf{k}_0\cdot\mathbf{L}_u + n\mathbf{k}_0\cdot\mathbf{L}_v - \mathbf{k}_s\cdot\mathbf{r}_{jmn} + \frac{k_0}{2r}[r_{jmn}^2 - (\hat{\mathbf{k}}_s\cdot\mathbf{r}_{jmn})^2] \tag{12}$$

$$\approx -\mathbf{k}_s\cdot\mathbf{r}_{j00} + m(\mathbf{k}_0-\mathbf{k}_s)\cdot\mathbf{L}_u + n(\mathbf{k}_0-\mathbf{k}_s)\cdot\mathbf{L}_v + \frac{1}{2k_0 r}[m^2(k_0^2 - k_{su}^0)L_u^2 + n^2(k_0^2-k_{sv}^2)L_v^2 + 2mn(k_0^2\mathbf{L}_u\cdot\mathbf{L}_v - k_{su}k_{sv}L_uL_v)] + O\left(\frac{mL}{r}\right), \tag{13}$$

where $k_{su}\equiv\mathbf{k}_s\cdot\mathbf{L}_u/L_u$, $k_{sv}\equiv\mathbf{k}_s\cdot\mathbf{L}_v/L_v$, and terms of order (mL/r) may be neglected because $mL/r\sim R_F/r\propto r^{-1/2}$ as $r\to\infty$. Thus, for $r\to\infty$, the electric field produced by the oscillating dipoles is

$$\mathbf{E}_s\left\{\frac{k_0^2}{r}\exp(ik_0 r)[1-\hat{\mathbf{k}}_s\hat{\mathbf{k}}_s]\sum_j\mathbf{P}_{j00}\exp(-i\mathbf{k}_s\cdot\mathbf{r}_{j00})\right\}G(r,\mathbf{k}_s), \tag{14}$$

$$G(r,\mathbf{k}_s) \equiv \sum_{m,n}\exp(i\Phi_{mn}), \tag{15}$$

$$\Phi_{mn} \equiv m(\mathbf{k}_0-\mathbf{k}_s)\cdot\mathbf{L}_u + n(\mathbf{k}_0-\mathbf{k}_s)\cdot\mathbf{L}_v + \frac{1}{2k_0 r}[m^2(k_0^2-k_{su}^2)L_u^2 + n^2(k_0^2-k_{sv}^2)L_v^2 + 2mn(k_0^2\mathbf{L}_u\cdot\mathbf{L}_v - k_{su}k_{sv}L_uL_v)]. \tag{16}$$

It is convenient to define

$$\mathbf{F}_{\rm TUC}(\hat{\mathbf{k}}_s) \equiv k_0^3[1-\hat{\mathbf{k}}_s\hat{\mathbf{k}}_s]\sum_{j=1}^{N}\mathbf{P}_{j00}\exp(i\omega t - i\mathbf{k}_s\cdot\mathbf{r}_{j00}), \tag{17}$$

so that the electric field produced by the dipoles is

$$\mathbf{E}_s = \frac{\exp(i\mathbf{k}_s\cdot\mathbf{r}-i\omega t)}{k_0 r}\mathbf{F}_{\rm TUC}(\hat{\mathbf{k}}_s)G(r,\mathbf{k}_s). \tag{18}$$

$\mathbf{F}_{\rm TUC}$ depends on the scattering direction $\hat{\mathbf{k}}_s$ and also on the direction of incidence $\hat{\mathbf{k}}_0$ and polarization $\mathbf{E}_0$ of the incident wave.

A. Isolated Finite Target: $\nu=0$

We will refer to finite isolated targets—consisting only of the dipoles in a single TUC—as targets that are periodic in $\nu=0$ dimensions. For this case, we simply set $G=1$ in Eq. (14); the scattered electric field in the radiation zone is

$$\mathbf{E}_s = \frac{\exp(ik_0 r - i\omega t)}{k_0 r}\mathbf{F}_{\rm TUC}(\hat{\mathbf{k}}_s). \tag{19}$$

The time-averaged scattered intensity is

$$I_s = \frac{c|\mathbf{E}_s|^2}{8\pi} = \frac{c}{8\pi k_0^2 r^2}|\mathbf{F}_{\rm TUC}|^2, \tag{20}$$

and the differential scattering cross section is

$$\frac{{\rm d}C_{\rm sca}}{{\rm d}\Omega} = \frac{1}{k_0^2}\frac{|\mathbf{F}_{\rm TUC}|^2}{|\mathbf{E}_0|^2}. \tag{21}$$

B. Target Periodic in One Dimension: $\nu=1$

Without loss of generality, we may assume that targets with 1-D periodicity repeat in the $\hat{\mathbf{y}}$ direction. It is easy to see from Eqs. (15) and (16) that $G=0$ except for scattering directions satisfying

$$k_{sy} = k_{0y} + M\frac{2\pi}{L_y} \qquad M = 0, \pm 1, \pm 2, \ldots, \tag{22}$$

where energy conservation ($k_s^2=k_0^2$) limits the allowed values of the integer M:

$$(-k_{0y}-k_0)\frac{L_y}{2\pi} \leqslant M \leqslant (-k_{0y}+k_0)\frac{L_y}{2\pi}. \tag{23}$$

If $(k_0+|k_{0y}|)L_y<2\pi$, then only $M=0$ scattering is allowed. Define polar angles α_0 and α_s for the incident and scattered radiation, so that

$$k_{0y} = k_0\cos\alpha_0, \tag{24}$$

$$k_{sy} = k_0\cos\alpha_s. \tag{25}$$

For each allowed value of k_{sy}, the scattering directions define a cone:

$$\mathbf{k}_s = k_{sy}\hat{\mathbf{y}} + (k_0^2-k_{sy}^2)^{1/2}\frac{\sin\alpha_s}{\sin\alpha_0}[(\hat{\mathbf{k}}_0 - \hat{\mathbf{y}}\cos\alpha_0)\cos\zeta + \hat{\mathbf{y}}\times\hat{\mathbf{k}}_0\sin\zeta], \tag{26}$$

where ζ is an azimuthal angle measured around the target axis $\hat{\mathbf{y}}$. The sum for $G(r,\mathbf{k}_s)$ is [since M must be an integer; see Eq. (22)]

$$G = \sum_{m=-\infty}^{\infty}\exp(i\Phi_{m0}) = \sum_{m=-\infty}^{\infty}\exp\left[-2\pi i M m + i\frac{m^2}{2k_0 r}(k_0^2-k_{sy}^2)L_y^2\right] \tag{27}$$

$$\to \lim_{\epsilon\to 0^+}\int_{-\infty}^{\infty}{\rm d}m\exp\left[\frac{i(1+i\epsilon)}{2k_0 r}m^2(k_0^2-k_{sy}^2)L_y^2\right] \tag{28}$$

$$= \frac{(2\pi i k_0 r)^{1/2}}{(k_0^2-k_{sy}^2)^{1/2}L_y} = \frac{(2\pi i k_0 r)^{1/2}}{k_0 L_y\sin\alpha_s}, \tag{29}$$

and the scattered electric field

$$\mathbf{E}_s = \left(\frac{2\pi i}{k_0 r}\right)^{1/2}\frac{\exp(ik_0 r - i\omega t)}{k_0 L_y\sin\alpha_s}\mathbf{F}_{\rm TUC}(\hat{\mathbf{k}}_s) \tag{30}$$

shows the expected $r^{-1/2}$ behavior far from the scatterer (the distance from the cylinder axis is $R=r\sin\alpha_s$).

For each allowed value of $\hat{\mathbf{k}}_s$, the total time-averaged scattered power $\bar{P}_{\rm sca}$, per unit length of the target, per unit azimuthal angle ζ, may be written

$$\frac{{\rm d}^2\bar{P}_{\rm sca}}{{\rm d}L{\rm d}\zeta} = \frac{|\mathbf{E}_0|^2}{8\pi}c\frac{{\rm d}^2C_{\rm sca}}{{\rm d}L{\rm d}\zeta}, \tag{31}$$

where the differential scattering cross section is

$$\frac{{\rm d}^2C_{\rm sca}}{{\rm d}L{\rm d}\zeta} = \frac{8\pi}{|\mathbf{E}_0|^2}\frac{1}{c}\frac{{\rm d}^2\bar{P}_{\rm sca}}{{\rm d}L{\rm d}\zeta} = \frac{8\pi}{|\mathbf{E}_0|^2 c}\frac{|\mathbf{E}|^2 c}{8\pi}R\sin\alpha_s \tag{32}$$

$$= \frac{2\pi}{k_0^3 L_y^2}\frac{|\mathbf{F}_{\rm TUC}|^2}{|\mathbf{E}_0|^2}. \tag{33}$$

C. Target Periodic in Two Dimensions: $\nu=2$

For targets that are periodic in two dimensions, it is apparent from Eqs. (15) and (16) that $G=0$ unless

$$(\mathbf{k}_s-\mathbf{k}_0)\cdot\mathbf{L}_u = 2\pi M, \qquad M = 0, \pm 1, \pm 2, \ldots, \tag{34}$$

$$(\mathbf{k}_s-\mathbf{k}_0)\cdot\mathbf{L}_v = 2\pi N, \qquad N = 0, \pm 1, \pm 2, \ldots. \tag{35}$$

The 2-D target constitutes a diffraction grating, with scattering allowed only in directions given by Eqs. (34) and (35). It is convenient to define the reciprocal lattice vectors

$$\mathbf{u} \equiv \frac{2\pi\hat{\mathbf{x}}\times\mathbf{L}_v}{\hat{\mathbf{x}}\cdot(\mathbf{L}_u\times\mathbf{L}_v)}, \quad \mathbf{v} \equiv \frac{2\pi\hat{\mathbf{x}}\times\mathbf{L}_u}{\hat{\mathbf{x}}\cdot(\mathbf{L}_v\times\mathbf{L}_u)}. \tag{36}$$

The wave vector transverse to the surface normal is

$$\mathbf{k}_{s\perp} \equiv \mathbf{k}_{0\perp} + M\mathbf{u} + N\mathbf{v}. \tag{37}$$

Energy conservation requires that

$$k_{sx}^2 = k_0^2 - |\mathbf{k}_{0\perp} + M\mathbf{u} + N\mathbf{v}|^2 > 0. \tag{38}$$

For any (M,N) allowed by Eq. (38), there are two allowed values of k_{sx} differing by a sign; one (with $k_{sx}k_{0x}>0$) corresponds to the (M,N) component of the transmitted wave, and the other (with $k_{sx}k_{0x}<0$) to the (M,N) component of the reflected wave. Define

$$\sin\alpha_0 \equiv \frac{|k_{0x}|}{k_0}, \tag{39}$$

$$\sin\alpha_s \equiv \frac{|k_{sx}|}{k_0}. \tag{40}$$

Note that $\alpha_0=\pi/2$ for normal incidence, and $\alpha_0\to 0$ for grazing incidence. For $\mathbf{k}_s$ satisfying Eqs. (34) and (35), we have

$$G = \sum_{m,n} \exp(i\Phi_{mn}) = \sum_{m,n} \exp\left\{ \frac{i}{2k_0 r}[(k_0^2 - k_{su}^2)L_u^2 m^2 + (k_0^2 - k_{sv}^2)L_v^2 n^2 + 2(k_0^2 \mathbf{L}_u \cdot \mathbf{L}_v - k_{su}k_{sv}L_u L_v)mn] \right\}$$

$$\to \lim_{\epsilon \to 0^+} \int_{-\infty}^{\infty} dm \int_{-\infty}^{\infty} dn \exp\left\{ \frac{i(1+i\epsilon)}{2k_0 r}[(k_0^2 - k_{su}^2)L_u^2 m^2 + k_0^2 - k_{sv}^2)L_v^2 n^2 + 2(k_0^2 \mathbf{L}_u \cdot \mathbf{L}_v - k_{su}k_{sv}L_u L_v)mn] \right\}$$

$$= \lim_{\epsilon \to 0^+} \frac{1}{A_{\mathrm{TUC}}} \int_{-\infty}^{\infty} dy \int_{-\infty}^{\infty} dz \exp\left\{ \frac{i(1+i\epsilon)}{2k_0 r}[k_0^2(y^2+z^2) - (k_{sy}y + k_{sz}z)^2] \right\} = \frac{2\pi i r}{k_0 A_{\mathrm{TUC}} \sin\alpha_s}. \quad (41)$$

The scattered electric field is

$$\mathbf{E}_s = \frac{2\pi i \exp(i\mathbf{k}_s \cdot \mathbf{r} - i\omega t)}{k_0^2 A_{\mathrm{TUC}} \sin\alpha_s} \mathbf{F}_{\mathrm{TUC}}(\hat{\mathbf{k}}_s). \quad (42)$$

Note that $|\mathbf{E}_s|$ is independent of distance $x = r\sin\alpha_s$ from the target, as expected for a target that is infinite in two directions. For pure forward scattering, $\mathbf{k}_s = \mathbf{k}_0$, we must sum the incident wave $\mathbf{E}_{\mathrm{inc}}$ and the radiated wave $\mathbf{E}_s$:

$$\mathbf{E} = \exp(i\mathbf{k}_0 \cdot \mathbf{r} - i\omega t)\left[\mathbf{E}_0 + \frac{2\pi i \mathbf{F}_{\mathrm{TUC}}(\hat{\mathbf{k}}_s = \hat{\mathbf{k}}_0)}{k_0^2 A_{\mathrm{TUC}} \sin\alpha_s} \right]. \quad (43)$$

The cross section per unit target area A for scattering into direction (M,N) is (for $\mathbf{k}_s \neq \mathbf{k}_0$)

$$\frac{dC_{\mathrm{sca}}(M,N)}{dA} = \frac{|\mathbf{E}|^2 \sin\alpha_s}{|\mathbf{E}_0|^2 \sin\alpha_0} \quad (44)$$

$$= \frac{4\pi^2}{k_0^4 A_{\mathrm{TUC}}^2 \sin\alpha_0 \sin\alpha_s} \frac{|\mathbf{F}_{\mathrm{TUC}}(\hat{\mathbf{k}}_s)|^2}{|\mathbf{E}_0|^2}, \quad (45)$$

where C_{sca} can be evaluated for either transmitted or reflected waves. For the special case $\mathbf{k}_s = \mathbf{k}_0$, the transmission coefficient $T(M,N)$ is obtained from the total forward-propagating wave (43):

$$T(0,0) = \frac{1}{|\mathbf{E}_0|^2} \left| \mathbf{E}_0 + \frac{2\pi i \mathbf{F}_{\mathrm{TUC}}(\hat{\mathbf{k}}_s = \hat{\mathbf{k}}_0)}{k_0^2 A_{\mathrm{TUC}} \sin\alpha_0} \right|^2. \quad (46)$$

4. SCATTERING AMPLITUDE MATRICES $S_i^{(\nu d)}$

A. Isolated Finite Targets: $\nu = 0$

In the radiation zone, the scattered electric field is related to the incident electric field via the 2×2 scattering amplitude matrix [16], defined so that

$$\begin{bmatrix} \mathbf{E}_s \cdot \hat{\mathbf{e}}_{s\parallel} \\ \mathbf{E}_s \cdot \hat{\mathbf{e}}_{s\perp} \end{bmatrix} = \frac{i \exp(i\mathbf{k}_s \cdot \mathbf{r} - i\omega t)}{k_0 r} \begin{bmatrix} S_2^{(0d)} & S_3^{(0d)} \\ S_4^{(0d)} & S_1^{(0d)} \end{bmatrix} \begin{bmatrix} \mathbf{E}_0 \cdot \hat{\mathbf{e}}_{i\parallel} \\ \mathbf{E}_0 \cdot \hat{\mathbf{e}}_{i\perp} \end{bmatrix}, \quad (47)$$

where

$$\hat{\mathbf{e}}_{i\perp} = \hat{\mathbf{e}}_{s\perp} \equiv \frac{\hat{\mathbf{k}}_s \times \hat{\mathbf{k}}_0}{|\hat{\mathbf{k}}_s \times \hat{\mathbf{k}}_0|} = \frac{\hat{\mathbf{k}}_s \times \hat{\mathbf{k}}_0}{1 - (\hat{\mathbf{k}}_s \cdot \hat{\mathbf{k}}_0)^2} = -\hat{\phi}_s, \quad (48)$$

$$\hat{\mathbf{e}}_{i\parallel} \equiv \hat{\mathbf{k}}_0 \times \hat{\mathbf{e}}_{i\perp} = \frac{\hat{\mathbf{k}}_s - (\hat{\mathbf{k}}_s \cdot \hat{\mathbf{k}}_0)\hat{\mathbf{k}}_0}{1 - (\hat{\mathbf{k}}_s \cdot \hat{\mathbf{k}}_0)^2}, \quad (49)$$

$$\hat{\mathbf{e}}_{s\parallel} \equiv \hat{\mathbf{k}}_s \times \hat{\mathbf{e}}_{s\perp} = \frac{-\hat{\mathbf{k}}_0 + (\hat{\mathbf{k}}_s \cdot \hat{\mathbf{k}}_0)\hat{\mathbf{k}}_s}{1 - (\hat{\mathbf{k}}_s \cdot \hat{\mathbf{k}}_0)^2} = \hat{\theta}_s \quad (50)$$

are the usual conventions for the incident and scattered polarization vectors parallel and perpendicular to the scattering plane (see, e.g., Sec. 3.2 of [16]).

B. Target Periodic in One Dimension: $\nu = 1$

For targets with 1-D periodicity, it is natural to generalize the scattering amplitude matrix, so that—for directions $\hat{\mathbf{k}}_s$ for which scattering is allowed—the scattered electric field at a distance $R = r\sin\alpha_s$ from the target is

$$\begin{bmatrix} \mathbf{E}_s \cdot \hat{\mathbf{e}}_{s\parallel} \\ \mathbf{E}_s \cdot \hat{\mathbf{e}}_{s\perp} \end{bmatrix} = \frac{i \exp(i\mathbf{k}_s \cdot \mathbf{r} - i\omega t)}{(k_0 R)^{1/2}} \begin{bmatrix} S_2^{(1d)} & S_3^{(1d)} \\ S_4^{(1d)} & S_1^{(1d)} \end{bmatrix} \begin{bmatrix} \mathbf{E}_0 \cdot \hat{\mathbf{e}}_{i\parallel} \\ \mathbf{E}_0 \cdot \hat{\mathbf{e}}_{i\perp} \end{bmatrix} \quad (51)$$

for $\mathbf{k}_s$ satisfying Eqs. (22)–(26).

C. Target Periodic in Two Dimensions: $\nu = 2$

For targets with 2-D periodicity, it is natural to generalize the scattering amplitude matrix so that, for directions $\mathbf{k}_s \neq \hat{\mathbf{k}}_0$ for which scattering is allowed, we write

$$\begin{bmatrix} \mathbf{E}_s \cdot \hat{\mathbf{e}}_{s\parallel} \\ \mathbf{E}_s \cdot \hat{\mathbf{e}}_{s\perp} \end{bmatrix} = i \exp(i\mathbf{k}_s \cdot \mathbf{r} - i\omega t) \begin{bmatrix} S_2^{(2d)} & S_3^{(2d)} \\ S_4^{(2d)} & S_1^{(2d)} \end{bmatrix} \begin{bmatrix} \mathbf{E}_0 \cdot \hat{\mathbf{e}}_{i\parallel} \\ \mathbf{E}_0 \cdot \hat{\mathbf{e}}_{i\perp} \end{bmatrix} \quad (52)$$

for $\mathbf{k}_s$ satisfying Eqs. (37) and (38).

For the special case of forward scattering ($M = N = 0$ and $\mathbf{k}_s = \mathbf{k}_0$), where the scattering plane is not simply defined by $\mathbf{k}_0$ and $\mathbf{k}_s$, it is natural to use $\mathbf{k}_0$ and the target normal $\hat{\mathbf{x}}$ to define the scattering plane. Thus

$$\hat{\mathbf{e}}_{i\perp} = \hat{\mathbf{e}}_{s\perp} \equiv \frac{\mathbf{k}_0 \times \mathbf{k}_{s\perp}}{|\mathbf{k}_0 \times \mathbf{k}_{s\perp}|}, \quad (53)$$

with $\hat{\mathbf{e}}_{i\parallel}$ and $\hat{\mathbf{e}}_{s\parallel}$ defined by Eqs. (49) and (50). For $r \to \infty$

$$\begin{bmatrix} \mathbf{E} \cdot \hat{\mathbf{e}}_{s\parallel} \\ \mathbf{E} \cdot \hat{\mathbf{e}}_{s\perp} \end{bmatrix} = i \exp(i\mathbf{k}_0 \cdot \mathbf{r} - i\omega t) \begin{bmatrix} (S_2^{(2d)} - i) & 0 \\ 0 & (S_1^{(2d)} - i) \end{bmatrix} \times \begin{bmatrix} \mathbf{E}_0 \cdot \hat{\mathbf{e}}_{i\parallel} \\ \mathbf{E}_0 \cdot \hat{\mathbf{e}}_{i\perp} \end{bmatrix}. \quad (54)$$

D. Far-Field Scattering Amplitude Matrices

The scattering amplitude matrices $S_i^{(\nu d)}(\mathbf{k}_s)$ are directly related to the $\mathbf{F}_{\mathrm{TUC}}$ for the three cases $\nu = 0, 1, 2$:

$$S_1^{(\nu d)} = C_\nu \hat{\mathbf{e}}_{s\perp} \cdot \mathbf{F}_{\mathrm{TUC}}(\hat{\mathbf{k}}_s, \mathbf{E}_0 = \hat{\mathbf{e}}_{i\perp}), \quad (55)$$

$$S_2^{(\nu d)} = C_\nu \hat{\mathbf{e}}_{s\parallel} \cdot \mathbf{F}_{\mathrm{TUC}}(\hat{\mathbf{k}}_s, \mathbf{E}_0 = \hat{\mathbf{e}}_{i\parallel}), \tag{56}$$

$$S_3^{(\nu d)} = C_\nu \hat{\mathbf{e}}_{s\parallel} \cdot \mathbf{F}_{\mathrm{TUC}}(\hat{\mathbf{k}}_s, \mathbf{E}_0 = \hat{\mathbf{e}}_{i\perp}), \tag{57}$$

$$S_4^{(\nu d)} = C_\nu \hat{\mathbf{e}}_{s\perp} \cdot \mathbf{F}_{\mathrm{TUC}}(\hat{\mathbf{k}}_s, \mathbf{E}_0 = \hat{\mathbf{e}}_{i\parallel}), \tag{58}$$

$$C_0 = -i, \tag{59}$$

$$C_1 = -\left(\frac{2\pi i}{\sin\alpha_s}\right)^{1/2} \frac{i}{k_0 L_y}, \tag{60}$$

$$C_2 = \frac{2\pi}{k_0^2 A_{\mathrm{TUC}} \sin\alpha_s}, \tag{61}$$

for finite targets (C_0) and targets that are periodic in one or two dimensions (C_1 or C_2).

5. FAR-FIELD SCATTERING MATRIX FOR STOKES VECTORS

For a given scattering direction $\hat{\mathbf{k}}_s$, the 2×2 complex amplitude matrix $S_i^{(\nu d)}(\mathbf{k}_s)$ fully characterizes the far-field scattering properties of the target. The far-field scattering properties of an isolated finite target are characterized by the 4×4 dimensionless Mueller matrix $S_{\alpha\beta}^{(0d)}$, with the Stokes vector of radiation scattered into direction $\hat{\mathbf{k}}_s$ at a distance r from the target given by

$$I_{\mathrm{sca},\alpha} \equiv \frac{1}{(k_0 r)^2} \sum_{\beta=1}^{4} S_{\alpha\beta}^{(0d)} I_{\mathrm{inc},\beta}, \tag{62}$$

where $I_{\mathrm{inc},\beta} = (I, Q, U, V)_{\mathrm{inc}}$ is the Stokes vector for the radiation incident on the target. For 1-D targets, we define the dimensionless scattering matrix $S_{\alpha\beta}^{(1d)}$ by

$$I_{\mathrm{sca},\alpha} \equiv \frac{1}{k_0 R} \sum_{\beta=1}^{4} S_{\alpha\beta}^{(1d)} I_{\mathrm{inc},\beta}, \tag{63}$$

where R is the distance from the 1-D target. For 2-D targets, we define $S_{\alpha\beta}^{(2d)}$ by

$$I_{\mathrm{sca},\alpha} \equiv \sum_{\beta=1}^{4} S_{\alpha\beta}^{(2d)} I_{\mathrm{inc},\beta}. \tag{64}$$

The 4×4 scattering intensity matrix $S_{\alpha\beta}^{(\nu d)}$ is obtained from the scattering amplitude matrix elements $S_i^{(\nu d)}$. Except for the special case of forward scattering ($\mathbf{k}_s = \mathbf{k}_0$) for 2-D targets, the equations are the same as Eq. (3.16) of Bohren and Huffman [16]. For example,

$$S_{11}^{(\nu d)} = \tfrac{1}{2}(|S_1^{(\nu d)}|^2 + |S_2^{(\nu d)}|^2 + |S_3^{(\nu d)}|^2 + |S_4^{(\nu d)}|^2), \tag{65}$$

$$S_{21}^{(\nu d)} = \tfrac{1}{2}(|S_2^{(\nu d)}|^2 - |S_1^{(\nu d)}|^2 - |S_4^{(\nu d)}|^2 + |S_3^{(\nu d)}|^2), \tag{66}$$

$$S_{14}^{(\nu d)} = \mathrm{Im}(S_2^{(\nu d)} S_3^{(\nu d)*} - S_1^{(\nu d)} S_4^{(\nu d)*}). \tag{67}$$

For the special case of forward scattering ($\hat{\mathbf{k}}_s = \hat{\mathbf{k}}_0$) for 2-D targets, it is necessary to replace $S_1^{(2d)}$ and $S_2^{(2d)}$ with $(S_1^{(2d)} - i)$ and $(S_2^{(2d)} - i)$ [cf. Eq. (54)]. Thus, for example,

$$S_{11}^{(2d)}(\mathbf{k}_s = \mathbf{k}_0) = \tfrac{1}{2}(|S_1^{(2d)} - i|^2 + |S_2^{(2d)} - i|^2 + |S_3^{(2d)}|^2 + |S_4^{(2d)}|^2). \tag{68}$$

6. TRANSMISSION AND REFLECTION COEFFICIENTS FOR 2-D TARGETS

For targets with 2-D periodicity, it is natural to define generalized transmission and reflection coefficients for the Stokes vectors: for scattering order (M,N), $I_{\mathrm{sca},\alpha} = \Sigma_\beta T_{\alpha\beta}(M,N) I_{\mathrm{inc},\beta}$ is the Stokes vector component α for radiation with $k_{sx} k_{\mathrm{inc},x} > 0$, and $R_{\alpha\beta}(M,N)$ is the fraction of the incident Stokes vector component β that emerges in Stokes vector component α with $k_{sx} k_{\mathrm{inc},x} < 0$. These can be related to the $S_{\alpha\beta}^{(2d)}$:

$$R_{\alpha\beta}(M,N) = \frac{\sin\alpha_s}{\sin\alpha_0} S_{\alpha\beta}^{(2d)} \qquad \text{for } k_{sx} k_{0x} < 0, \tag{69}$$

$$T_{\alpha\beta}(M,N) = \frac{\sin\alpha_s}{\sin\alpha_0} S_{\alpha\beta}^{(2d)} \qquad \text{for } k_{sx} k_{0x} > 0. \tag{70}$$

The fraction of the incident power that is absorbed by the target is

$$\frac{P_{\mathrm{abs}}/\mathrm{Area}}{|\mathbf{E}_0|^2 c \sin\alpha_0/8\pi} = 1 - \sum_{M,N} \sum_{\beta=1}^{4} [R_{1\beta}(M,N) + T_{1\beta}(M,N)] \frac{I_{\mathrm{inc},\beta}}{I_{\mathrm{inc},1}}, \tag{71}$$

where $I_{\mathrm{inc},\beta}$ is the Stokes vector of the incident radiation.

For unpolarized incident radiation, $R_{11}(M,N)$ is the fraction of the incident power that is reflected in diffraction component (M,N), $T_{11}(M,N)$ is the fraction that is transmitted in component (M,N), and $1 - \Sigma_{M,N}[R_{11}(M,N) + T_{11}(M,N)]$ is the fraction of the incident power that is absorbed.

7. EXAMPLE: INFINITE CYLINDER

DDSCAT 7 has been used to calculate scattering and absorption by an infinite cylinder consisting of a periodic array of disks of thickness d and period $L_y = d$ (where d is the interdipole spacing). Figure 3(a) shows $S_{11}^{(1d)}$ for refractive index $m = 1.33 + 0.01i$, $\pi D/\lambda = 50$ (D is the cylinder diameter and λ the wavelength of the incident radiation), and incidence angle $\alpha_0 = 60°$. Because $k_0(1 + |\cos\alpha_0|)d < 2\pi$, Eqs. (22) and (23) allow only $M = 0$ scattering, with $\alpha_s = \alpha_0$. Also shown is the exact solution, calculated using a code written by Mackowski [17]. Light scattering by cylinders is generally described by scattering amplitudes T_i; in Appendix B we provide expressions relating these T_i to the S_i used here. Figure 3(b) shows the fractional error in $S_{11}^{(1d)}$ calculated using DDSCAT. As d is decreased, the errors decrease. Excellent accuracy is obtained when the validity criterion [3] $|m|kd \lesssim 0.5$ is satisfied: the fractional error in S_{11} is typically less than a few%, except near deep minima in S_{11}.

Figure 3(c) shows $S_{21}^{(1d)}$, characterizing scattering of unpolarized light into the Stokes parameter Q ($S_{21} < 0$ corresponds to linear polarization perpendicular to the scattering plane). DDSCAT 7 and the exact solution are in very

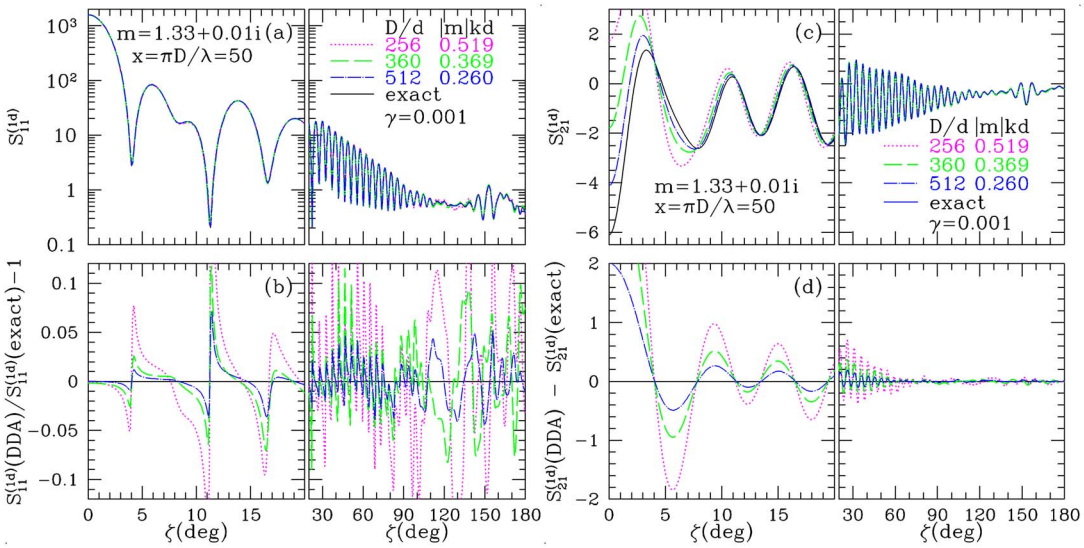

Fig. 3. (Color online) Scattering by an infinite cylinder with diameter D and $m=1.33+0.01i$, for radiation with $x=\pi D/\lambda=50$ and incidence angle $\alpha_0=60°$. (a) $S_{11}^{(1d)}$: solid curve, exact solution; broken curves, DDA results for $D/d=256$, 360, and 512 ($N=51{,}676$, 102,036, 206,300 dipoles per TUC). (b) Fractional error in $S_{11}^{(1d)}$(DDA). (c) $S_{21}^{(1d)}$. (d) Error in $S_{21}^{(1d)}$.

good agreement when $|m|kd \lesssim 0.5$. Note that although the error in $S_{21}^{(1d)}(\theta=0)\approx 2$ is large compared to $S_{21}(0)=-6$, this is small compared to $S_{11}^{(1d)}(0)\approx 1500$: the scattered radiation is only slightly polarized.

The results in Fig. 3 were obtained using $\gamma=0.001$ to truncate the integrations. To see how the results depend on γ, Fig. 4 shows $S_{11}^{(1d)}$ computed for the problem of Fig. 3 but using different values of γ. For azimuthal angles $\zeta > 20°$, the results for $\gamma=0.005$ and 0.001 are nearly indistinguishable; the difference between the computed result and the exact solution is evidently due to the finite number of dipoles used, rather than the choice of cutoff parameter γ. However, the results for forward scattering are more sensitive to the choice of γ, as is seen in Figs. 4(c) and 4(d): it is necessary to reduce γ to 0.001 to attain high accuracy in the forward-scattering directions.

Table 1 gives the CPU times to calculate $\tilde{\mathbf{A}}$, to then iteratively solve the scattering problem to a fractional error $<10^{-5}$ (using double-precision arithmetic), and finally to evaluate the scattering intensities for several of the cases shown in Figs. 3 and 4. For most cases the CPU time is dominated by the iterative solution using the conjugate gradient algorithm. While the time required to evaluate $\tilde{\mathbf{A}}$ might be reduced using the strategies suggested by [10], this step is generally a subdominant part of the computation for targets with $kd \gtrsim 0.1$.

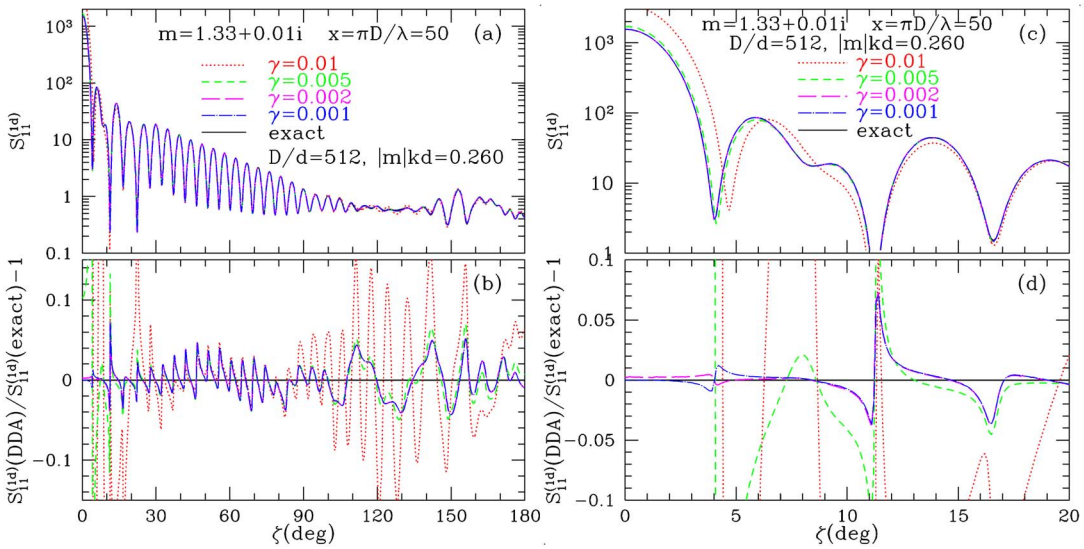

Fig. 4. (Color online) Scattering by an infinite cylinder with diameter D and $m=1.33+0.01i$, for radiation with $\pi D/\lambda=50$ and incidence angle $\alpha_0=60°$. (a) Exact solution (solid curve) and DDA results for $D/d=512$ and various values of the interaction cutoff parameter γ. (b) Fractional error in $S_{11}^{(1d)}$. (c), (d) Same as (a), (b), but expanding the region $0<\zeta<20°$. For this case, results computed with $\gamma=0.002$ and 0.001 are nearly indistinguishable.

Table 1. CPU Time to Calculate Scattering by $m=1.33+0.01i$ Infinite Cylinders on Single-Core 2.4 GHz AMD Opteron Model 250

$\pi D/\lambda$	N	γ	Calc. $\tilde{\mathbf{A}}$ (min)	Solution (min)	Scat. (min)	Total (min)
25	51,676	0.005	3.29	17.6	0.65	22.2
25	51,676	0.001	16.2	17.8	0.65	35.3
50	102,036	0.005	4.58	59.7	1.27	66.8
50	102,036	0.001	22.8	45.2	1.09	70.2
50	206,300	0.005	13.2	254	2.88	273
50	206,300	0.001	66.0	292	2.76	364

The above results have been for a weakly absorbing cylinder. To confirm that the DDA can be applied to strongly absorbing material, Fig. 5 shows scattering calculated for a cylinder with $m=2+i$ and $x=\pi D/\lambda=25$. Once again, the accuracy is very good, with small fractional errors provided $|m|kd\lesssim 0.5$.

8. EXAMPLE: PLANE-PARALLEL SLAB

Consider a homogeneous plane-parallel slab with thickness h and refractive index m. Radiation incident on it at angle of incidence θ_i will either be specularly reflected or transmitted. The reflection and transmission coefficients R and T can be calculated analytically, taking into account multiple reflections within the slab [15]. With an exact solution in hand, we can evaluate the accuracy of the DDA applied to this problem. Figure 6 shows results for two cases: a dielectric slab with $m=1.50$, and an absorbing slab with $m=1.50+0.02i$.

DDSCAT 7 was used to calculate reflection, transmission, and absorption by an infinite slab, generated from a TUC consisting of a single line of dipoles extending in the x direction, with $L_y=L_z=d$. The selection rules (34), (35), and (38) allow only $M=N=0$: transmission or specular reflection. The reflection and transmission coefficients for radiation polarized parallel or perpendicular to the plane containing $\hat{\mathbf{k}}$ and the surface normal are

$$R_{\parallel}=S_{11}^{(1d)}(k_{sx}=-k_{0x})+S_{12}^{(1d)}(k_{sx}=k_{0x}), \tag{72}$$

$$R_{\perp}=S_{11}^{(1d)}(k_{sx}=-k_{0x})-S_{12}^{(1d)}(k_{sx}=k_{0x}), \tag{73}$$

$$T_{\parallel}=S_{11}^{(1d)}(k_{sx}=k_{0x})+S_{12}^{(1d)}(k_{sx}=k_{0x}), \tag{74}$$

$$T_{\perp}=S_{11}^{(1d)}(k_{sx}=k_{0x})-S_{12}^{(1d)}(k_{sx}=k_{0x}). \tag{75}$$

The DDA results are in excellent agreement with the exact results when the validity condition $|m|k_0d<0.5$ is satisfied, but results with moderate accuracy are obtained even when $|m|k_0d\approx 1$.

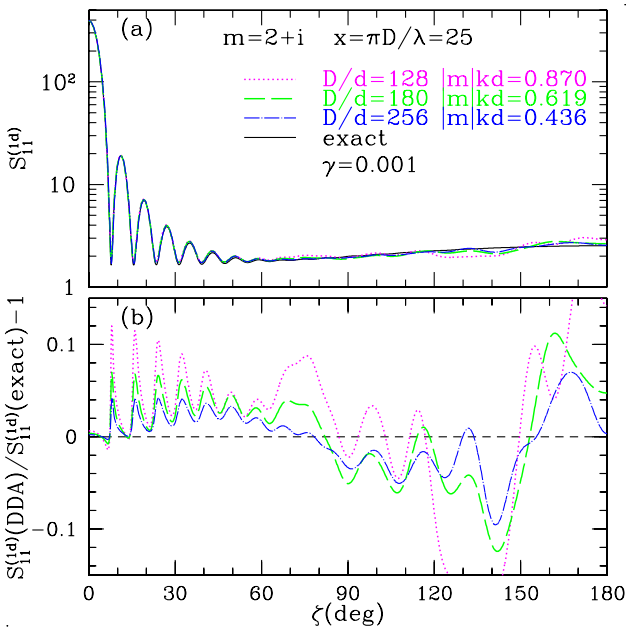

Fig. 5. (Color online) Light scattered by an infinite cylinder with $m=2+i$ for radiation with $x=2\pi R/\lambda=25$ and incidence angle $\alpha_0=60°$. (a) $S_{11}^{(1d)}$: solid curve, exact solution; broken curves, DDA results for $D/d=128$, 180, and 256 ($N=12{,}972$, 25,600, 51,676 dipoles per TUC). (b) Fractional error in $S_{11}^{(1d)}$.

9. NEAR-FIELD EVALUATION

The polarizations $\mathbf{P}_{j00}$ can be used to calculate the electric and magnetic fields at any point, including within or near the target, using the exact expression for $\mathbf{E}$ and $\mathbf{B}$ from a point dipole, modified by a function ϕ:

$$\mathbf{E}(\mathbf{r},t)=e^{-i\omega t}\sum_j\sum_{m,n}{}'\frac{\exp(ik_0R_{jmn})}{|R_{jmn}|^3}\phi(R_{jmn})\Bigg\{k_0^2\mathbf{R}_{jmn}\times(\mathbf{P}_{jmn}\times\mathbf{R}_{jmn})+\frac{(1-ik_0R_{jmn})}{R_{jmn}^2}[3\mathbf{R}_{jmn}(\mathbf{R}_{jmn}\cdot\mathbf{P}_{jmn})-R_{jmn}^2\mathbf{P}_{jmn}]\Bigg\}+\mathbf{E}_0\exp(i\mathbf{k}_0\cdot\mathbf{r}-i\omega t), \tag{76}$$

$$\mathbf{B}(\mathbf{r},t)=e^{-i\omega t}\sum_j\sum_{m,n}{}'k^2\frac{\exp(ik_0R_{jmn})}{R_{jmn}^2}\phi(R_{jmn})(\mathbf{R}_{jmn}\times\mathbf{P}_{jmn})\times\left(1-\frac{1}{ik_0R_{jmn}}\right)+\hat{\mathbf{k}}_0\times\mathbf{E}_0\exp(i\mathbf{k}_0\cdot\mathbf{r}-i\omega t), \tag{77}$$

$$\mathbf{R}_{jmn}\equiv\mathbf{r}-\mathbf{r}_{jmn}, \tag{78}$$

$$\phi(R)\equiv\exp[-\gamma(k_0R)^4]\times\begin{cases}1 & \text{for } R\geq d\\ (R/d)^4 & \text{for } R<d\end{cases}. \tag{79}$$

The function $\phi(R)$ smoothly suppresses the (oscillating) contribution from distant dipoles in order to allow the summations to be truncated, just as in Eq. (6) for evaluation of $\tilde{\mathbf{A}}_{j,k}$. If $\mathbf{r}$ is within the target or near the target surface, the summations over (m,n) are limited to $|R_{jmn}|\leq 2/\gamma k_0$. The $(R/d)^4$ factor suppresses the R^{-3} divergence of $\mathbf{E}$ as $\mathbf{r}$ approaches the locations of individual dipoles, and at the dipole locations results in $\mathbf{E}$ that is exactly equal to the field that is polarizing the dipoles in the DDA formulation. Evaluation of Eqs. (76) and (77) is computationally intensive, because the summations $\Sigma_j\Sigma'_{m,n}$ typically have many terms.

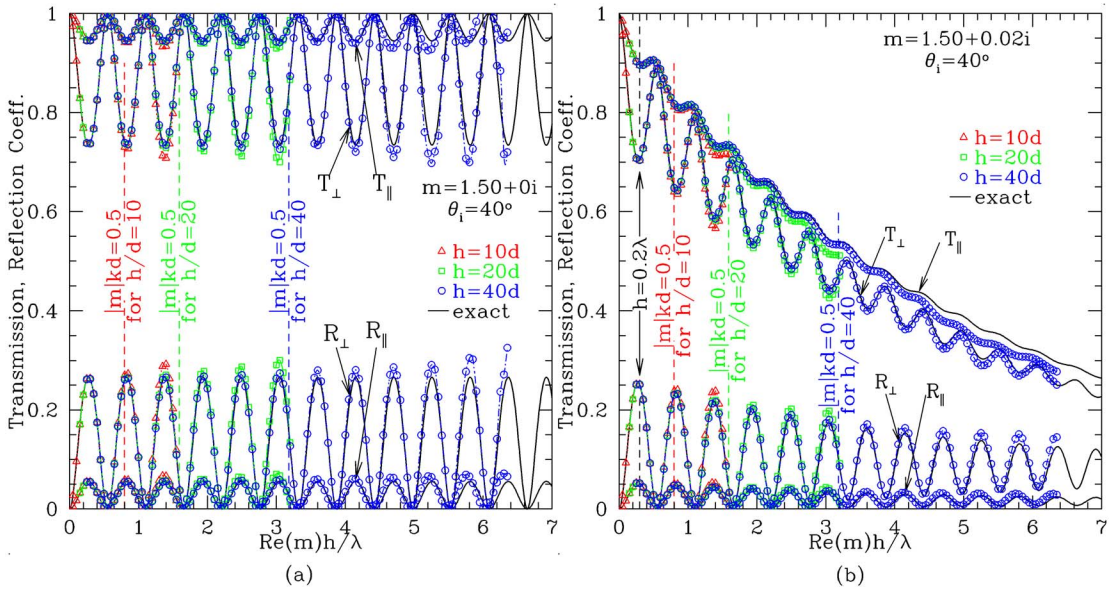

Fig. 6. (Color online) Transmission and reflection coefficients for radiation of wavelength λ incident at angle $\theta_i=(\pi/2-\alpha_0)=40°$ relative to the normal on a slab with thickness h, incident $\mathbf{E}\parallel$ and $\perp$ to the scattering plane, as a function of $\mathrm{Re}(m)h/\lambda$. (a) Nonabsorbing slab with $m=1.5$. (b) Absorbing slab with $m=1.5+0.02i$. Solid curves exact solution; symbols, results calculated with the DDA using dipole spacing $d=h/10$, $h/20$, and $h/40$.

To illustrate the accuracy, we consider the infinite slab of Fig. 6(b), with refractive index $m=1.5+0.02i$ and radiation incident at an angle $\theta_i=40°$. Figure 7 shows the time-averaged $|\mathbf{E}|^2/|\mathbf{E}_0|^2$ for slab thickness $h=0.2\lambda$—near a minimum in transmission, and a maximum in reflection [see Fig. 6(b)]. The program DDFIELD (see Appendix A) was used to evaluate $\mathbf{E}$ along two lines normal to the slab: track 1 passes directly through dipole sites, and track 2 passes midway between the four nearest dipoles as it crosses each dipole layer. The E fields calculated along tracks 1 and 2 are very similar, although of course not identical. Within the slab, $|\mathbf{E}|$ along track 2 tends to be slightly smaller than along track 1, but for this example the difference is typically less than ~1%. Figure 7 shows results for the slab represented by $h/d=N_x=10$ and 20 dipole layers (with $|m|kd=0.19$ and 0.094, respectively).

Even for $N_x=10$, the electric field at points more than a distance d from the edge is obtained to within ~2% accuracy at worst, which is perhaps not surprising because, as seen in Fig. 6, the calculated transmission and reflection coefficients are very accurate. The discontinuity in $|E|^2$ at the boundary is spread out over a distance ~d. The DDA

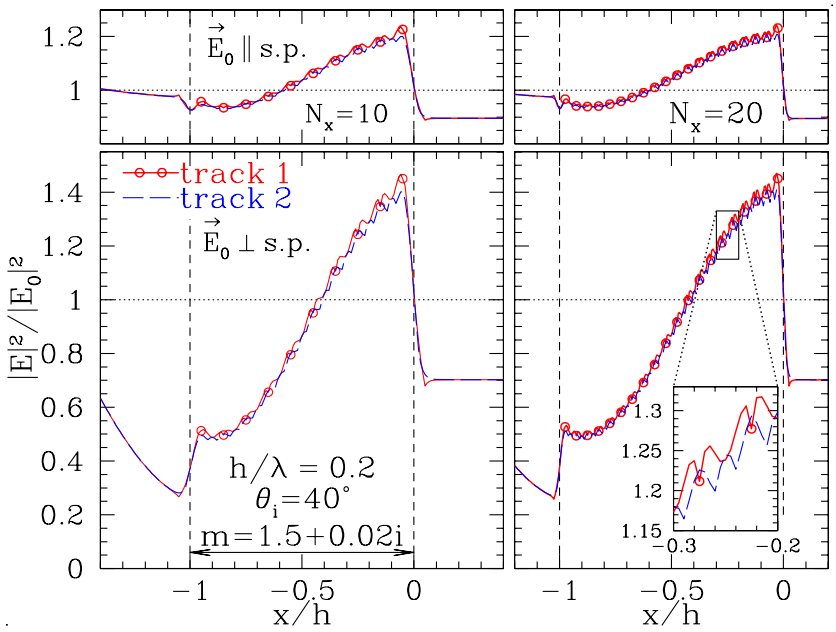

Fig. 7. (Color online) $|\mathbf{E}^2|/|\mathbf{E}_0^2|$ within and near the dielectric slab of Fig. 6(b) for slab thickness $h=0.2\lambda$, incidence angle $\alpha_i=40°$, and incident polarizations $\parallel$ and $\perp$ to the scattering plane. Results were calculated using Eq. (76) with the slab represented by $N_x=10$ and $N_x=20$ dipole layers (i.e., dipole spacing $d=0.1h$ and $0.05h$). The circles along track 1 are at points where dipoles are located.

obviously cannot reproduce field structure near the target surface on scales smaller than the dipole separation d, but fields on scales larger than d appear to be quite accurate. DDSCAT and DDFIELD should be useful tools for studying electromagnetic fields around arrays of nanostructures, such as gold nanodisks [18,19].

10. SUMMARY

The principal results of this study are as follows:

1. The DDA is generalized to treat targets that are periodic in one or two spatial dimensions. Scattering and absorption of monochromatic plane waves can be calculated using algorithms that parallel those used for finite targets.
2. A general formalism is presented for description of far-field scattering by targets that are periodic in one or two dimensions using scattering amplitude matrices and Mueller matrices that are similar in form to those for finite targets.
3. The accuracy of the DDA for periodic targets is tested for two examples: infinite cylinders and infinite slabs. The DDA, as implemented in DDSCAT 7, is accurate provided the validity criterion $|m|kd \lesssim 0.5$ is satisfied.
4. We show how the DDA solution can be used to evaluate **E** and **B** within and near the target, with calculations for an infinite slab used to illustrate the accuracy of near-field calculations.

APPENDIX A: DDSCAT 7 AND DDFIELD

The theoretical developments reported here have been implemented in a new version of the open-source code DDSCAT [20]. DDSCAT 7 is written in Fortran 90 with dynamic memory allocation and the option to use either single- or double-precision arithmetic. DDSCAT 7 includes options for various target geometries, including a number of periodic structures. A program DDFIELD for near-field calculations is also provided.

DDSCAT 7 offers the option of using an implementation of BICGSTAB with enhancement to maintain convergence in finite precision arithmetic [21]. The matrix-vector multiplications $\tilde{\mathbf{A}}\mathbf{P}$ are accomplished efficiently using FFTs [22]. Documentation for DDSCAT is available from ArXiv [23], with additional information available from [24].

In addition to differential scattering cross sections, DDSCAT reports dimensionless "efficiency factors" $Q_x \equiv C_x(\mathrm{TUC})/\pi a_{\mathrm{eff}}^2$ for scattering and absorption, where $C_x(\mathrm{TUC})$ is the total cross section for scattering or absorption per TUC, normalized by πa_{eff}^2, where $a_{\mathrm{eff}} \equiv (3V_{\mathrm{TUC}}/4\pi)^{1/3}$ is the radius of a sphere with volume equal to the solid volume V_{TUC} in one TUC.

In the case of 1-D targets with periodicity L_y in the y direction, the absorption, scattering, and extinction cross sections per unit target length are

$$\frac{dC_x}{dL} = \frac{1}{L_y} Q_x \pi a_{\mathrm{eff}}^2 \tag{A1}$$

for $x = $ ext, sca, and abs, where Q_x are the efficiency factors calculated by DDSCAT.

In the case of 2-D targets with periodicities L_u and L_v, the absorption, scattering, and extinction cross sections per unit target area are

$$\frac{dC_x}{dA} = \frac{Q_x \pi a_{\mathrm{eff}}^2}{L_u L_v \sin\theta_{uv}}. \tag{A2}$$

APPENDIX B: RELATION BETWEEN S_i AND T_i FOR INFINITE CYLINDERS

The analytic solution for infinite cylinders decomposes the incident and scattered radiation into components polarized parallel and perpendicular to planes containing the cylinder axis and the propagation vector $\hat{\mathbf{k}}_0$ or $\hat{\mathbf{k}}_s$. These polarization basis states differ from the choice that is usual for scattering by finite particles, where it is customary to decompose the incident and scattered waves into components polarized parallel and perpendicular to the *scattering* plane—the plane containing $\hat{\mathbf{k}}_0$ and $\hat{\mathbf{k}}_s$.

In the notation of Bohren and Huffman [16], the radiation scattered by an infinite cylinder can be written

$$\begin{bmatrix} \mathbf{E}_s \cdot \hat{\mathbf{e}}_{s\parallel}^{(ck)} \\ \mathbf{E}_s \cdot \hat{\mathbf{e}}_{s\perp}^{(ck)} \end{bmatrix} = i \exp(i\mathbf{k}_s \cdot \mathbf{r} - i\omega t) \left(\frac{2i}{\pi k_0 R \sin\alpha} \right)^{1/2} \begin{bmatrix} T_1 & -T_3 \\ T_3 & T_2 \end{bmatrix} \times \begin{bmatrix} \mathbf{E}_0 \cdot \hat{\mathbf{e}}_{i\parallel}^{(ck)} \\ \mathbf{E}_0 \cdot \hat{\mathbf{e}}_{i\perp}^{(ck)} \end{bmatrix}, \tag{B1}$$

where R is the distance from the cylinder axis, α is the angle between $\mathbf{k}_0$ and the cylinder axis c, and superscript (ck) denotes polarization vectors parallel or perpendicular to planes containing the cylinder axis $\hat{\mathbf{c}}$ and either $\mathbf{k}_0$ or $\mathbf{k}_s$. The azimuthal angle ζ is measured around the cylinder axis $\hat{\mathbf{c}}$, with $\zeta = 0$ for forward scattering. The scattering angle $\theta = \arccos[\hat{\mathbf{k}}_0 \cdot \hat{\mathbf{k}}_s]$ is

$$\theta = \arccos[1 - (1 - \cos\zeta)\sin^2\alpha]. \tag{B2}$$

The scattering amplitude matrix elements T_i appearing in Eq. (B1) can be related to the matrix elements S_i appearing in Eq. (51):

$$\mathbf{S} = \left(\frac{2i}{\pi \sin\alpha} \right)^{1/2} \mathbf{A}\mathbf{T}\mathbf{B}^{-1}, \tag{B3}$$

$$\mathbf{S} \equiv \begin{bmatrix} S_2^{(1d)} & S_3^{(1d)} \\ S_4^{(1d)} & S_1^{(1d)} \end{bmatrix}, \quad \mathbf{T} \equiv \begin{bmatrix} T_1 & -T_3 \\ T_3 & T_2 \end{bmatrix}, \tag{B4}$$

$$\mathbf{A} \equiv \begin{bmatrix} \hat{\mathbf{e}}_{s\parallel} \cdot \hat{\mathbf{e}}_{s\parallel}^{(ck)} & \hat{\mathbf{e}}_{s\parallel} \cdot \hat{\mathbf{e}}_{s\perp}^{(ck)} \\ \hat{\mathbf{e}}_{s\perp} \cdot \hat{\mathbf{e}}_{s\parallel}^{(ck)} & \hat{\mathbf{e}}_{s\perp} \cdot \hat{\mathbf{e}}_{s\perp}^{(ck)} \end{bmatrix} = \frac{1}{\sin\theta} \begin{bmatrix} -\cot\alpha(1-\cos\theta) & \sin\alpha\sin\zeta \\ -\sin\alpha\sin\zeta & -\cot\alpha(1-\cos\theta) \end{bmatrix}, \tag{B5}$$

$$\mathbf{B} \equiv \begin{bmatrix} \hat{\mathbf{e}}_{i\parallel} \cdot \hat{\mathbf{e}}_{i\parallel}^{(ck)} & \hat{\mathbf{e}}_{i\parallel} \cdot \hat{\mathbf{e}}_{i\perp}^{(ck)} \\ \hat{\mathbf{e}}_{i\perp} \cdot \hat{\mathbf{e}}_{i\parallel}^{(ck)} & \hat{\mathbf{e}}_{i\perp} \cdot \hat{\mathbf{e}}_{i\perp}^{(ck)} \end{bmatrix} = \frac{1}{\sin\theta} \begin{bmatrix} \cot\alpha(1-\cos\theta) & \sin\alpha\sin\zeta \\ -\sin\alpha\sin\zeta & \cot\alpha(1-\cos\theta) \end{bmatrix}, \tag{B6}$$

$$\mathbf{B}^{-1} = \frac{\sin\theta}{\cot^2\alpha(1-\cos\theta)^2 + \sin^2\alpha\sin^2\zeta} \times \begin{bmatrix} \cot\alpha(1-\cos\theta) & -\sin\alpha\sin\zeta \\ \sin\alpha\sin\zeta & \cot\alpha(1-\cos\theta) \end{bmatrix}. \quad \text{(B7)}$$

ACKNOWLEDGMENTS

This research was supported in part by National Science Foundation (NSF) grant AST-0406883, and by the Office of Naval Research (ONR). We thank Dan Mackowski for providing his code for light scattering by infinite cylinders, H. A. Yousif for discussions concerning scattering by infinite cylinders, and the referees for helpful comments.

REFERENCES

1. E. M. Purcell and C. R. Pennypacker, "Scattering and absorption of light by nonspherical dielectric grains," Astrophys. J. **186**, 705–714 (1973).
2. B. T. Draine, "The discrete-dipole approximation and its application to interstellar graphite grains," Astrophys. J. **333**, 848–872 (1988).
3. B. T. Draine and P. Flatau, "Discrete-dipole approximation for scattering calculations," J. Opt. Soc. Am. A **11**, 1491–1499 (1994).
4. B. T. Draine, "The discrete dipole approximation for light scattering by irregular targets," in *Light Scattering by Nonspherical Particles: Theory, Measurements, and Applications*, M. I. Mishchenko, J. W. Hovenier, and L. D. Travis, eds. (Academic, 2000), pp. 131–145.
5. R. Schmehl, B. M. Nebeker, and E. D. Hirleman, "Discrete-dipole approximation for scattering by features on surfaces by means of a two-dimensional fast Fourier transform technique," J. Opt. Soc. Am. A **14**, 3026–3036 (1997).
6. M. Paulus and O. J. F. Martin, "Green's tensor technique for scattering in two-dimensional stratified media," Phys. Rev. E **63**, 066615 (2001).
7. P. Yang and K. N. Liou, "Finite difference time domain method for light scattering by nonspherical and inhomogeneous particles," in *Light Scattering by Nonspherical Particles: Theory, Measurements, and Applications*, M. I. Mishchenko, J. W. Hovenier, and L. D. Travis, eds. (Academic, 2000), pp. 173–221.
8. A. Taflove and S. C. Hagness, *Advances in Computational Electrodynamics: the Finite-Difference Time-Domain Method* (Artech House, 2005).
9. V. A. Markel, "Coupled-dipole approach to scattering of light from a one-dimensional periodic dipole structure," J. Mod. Opt. **40**, 2281–2291 (1993).
10. P. C. Chaumet, A. Rahmani, and G. W. Bryant, "Generalization of the coupled dipole method to periodic structures," Phys. Rev. B **67**, 165404 (2003).
11. P. C. Chaumet and A. Sentenac, "Numerical simulations of the electromagnetic field scattered by defects in a double-periodic structure," Phys. Rev. B **72**, 205437 (2005).
12. B. T. Draine and P. Flatau, "User Guide for the Discrete Dipole Approximation Code DDSCAT6.1," http://arXiv.org/abs/astro-ph/0409262 (2004).
13. B. T. Draine and J. Goodman, "Beyond Clausius-Mossotti—Wave propagation on a polarizable point lattice and the discrete dipole approximation," Astrophys. J. **405**, 685–697 (1993).
14. D. Gutkowicz-Krusin and B. T. Draine, "Propagation of electromagnetic waves on a rectangular lattice of polarizable points," http://arXiv.org/abs/astro-ph/0403082 (2004).
15. M. Born and E. Wolf, *Principles of Optics* (Cambridge U. Press, 1999).
16. C. F. Bohren and D. R. Huffman, *Absorption and Scattering of Light by Small Particles* (Wiley, 1983).
17. D. Mackowski, private communication (2007).
18. Z. N. Utegulov, J. M. Shaw, B. T. Draine, S. A. Kim, and W. L. Johnson, "Surface-plasmon enhancement of Brillouin light scattering from gold-nanodisk arrays on glass," Proc. SPIE **6641**, 66411M (2007).
19. W. L. Johnson, S. A. Kim, Z. N. Utegulov, and B. T. Draine, "Surface-plasmon fields in two-dimensional arrays of gold nanodisks," Proc. SPIE **7032** (2008) (to be published).
20. http://www.astro.princeton.edu/~draine/DDSCAT.html (2008).
21. M. A. Botchev, SUBROUTINE ZBCG2, http://www.math.uu.nl/people/vorst/zbcg2.f90 (2001).
22. J. J. Goodman, B. T. Draine, and P. J. Flatau, "Application of fast-Fourier transform techniques to the discrete dipole approximation," Opt. Lett. **16**, 1198–1200 (1990).
23. B. T. Draine and P. Flatau, "User Guide for the Discrete Dipole Approximation Code DDSCAT 7.0," http://arXiv.org/abs/0809.0337 (2008).
24. http://ddscat.wikidot.com.